Applied Catalysis B: Environmental 255 (2019) 117754

Contents lists available at ScienceDirect

Applied Catalysis B: Environmental

journal homepage: www.elsevier.com/locate/apcatb

Role of surface reconstruction on Cu/TiO_2 nanotubes for CO_2 conversion

Chao Liu[a], Scott L. Nauert[b], Marco A. Alsina[a], Dingdi Wang[c], Alexander Grant[b], Kai He[d], Eric Weitz[c,*], Michael Nolan[e], Kimberly A. Gray[a,*], Justin M. Notestein[b,*]

[a] Department of Civil and Environmental Engineering, Northwestern University, Evanston, IL, 60208, United States
[b] Department of Chemical and Biological Engineering, Northwestern University, Evanston, IL, 60208, United States
[c] Department of Chemistry, Northwestern University, Evanston, IL, 60208, United States
[d] Department of Materials Science and Engineering, Northwestern University, Evanston, IL, 60208, United States
[e] Tyndall National Institute, University College Cork, Lee Maltings, Cork, Ireland

ARTICLE INFO

Keywords:
Reverse water-gas shift
SMSI
Supported metals
CO_2 conversion
Spectroscopy

ABSTRACT

Carbon dioxide hydrogenation to CO via the reverse water gas shift (RWGS) reaction is one route to integrate CO_2 utilization into the chemical industry. TiO_2 supported Cu catalysts are known to be active for RWGS, but Cu is shown here to behave differently on TiO_2 nanotubes (TiNT) vs TiO_2 nanoparticles (TiNP). Whereas nanoparticle supports give low rates that are hardly changed by added Cu, the nanotube supports yield much higher activity and three distinct behaviors as the Cu surface density increases. At low surface densities (0.3 Cu/nm^2), active Cu-O-Ti sites are created that have low apparent activation energies. At high surface densities (6 Cu/nm^2), Cu nanoparticles on TiNT are formed, and reaction barriers are lowered when both Cu and TiNT surfaces are accessible. At intermediate surface densities, metallic Cu domains are engulfed by a TiOx overlayer formed during H_2 pretreatment, akin to those formed by classical strong metal support interactions (SMSI). These reduced layers are markedly more active for RWGS than the initial TiNT surfaces, but have similar activation barriers, which are higher than those for which both Cu and TiNP surfaces are exposed. These catalytic findings are supported by computational modeling, *in situ* IR, UV–vis, and X-ray absorption spectroscopies, and they provide insight into an important reaction for CO_2 utilization.

1. Introduction

Conversion of CO_2 to feedstock chemicals is a key step in remaking the value chain and creating carbon neutral cycles in the chemical industry [1,2] The water gas shift and reverse water gas shift (RWGS) reactions ($CO + H_2O \leftrightarrow CO_2 + H_2$) are well-known and widely utilized in industry to adjust the ratios of CO and H_2 in syngas for the Fischer-Tropsch process [3,4]. RWGS is endothermic and thermodynamically favored at elevated temperature [5], making it an inevitable reaction during any CO_2 hydrogenation process. For example, Rodriguez et al. found that RWGS and methanol synthesis have similar apparent activation energies on a Cu/CeOx catalyst [6].

Cu catalysts are considered as among the more promising catalysts for RWGS since CO, the product, does not interact strongly with metallic Cu [7]. TiO_2 supported Cu catalysts have been reported to catalyze the conversion of CO_2 to CO, methane and methanol [8–11]. A potential complicating factor in understanding these materials is the requirement to activate the catalysts in H_2 to form metallic or low oxidation state Cu species [12–23], create oxygen vacancies or undercoordinated Ti sites on TiO_2 [22,23], and to remove carbonaceous species [15]. Although metal nanoparticles on TiO_2 and other reducible supports are well known to reconstruct in reducing environments [24–26], the potential role of the surface reconstruction of Cu/TiO_2 catalysts in CO_2 conversion reactions is not well understood.

TiO_2 nanotubes (TiNT), with their unique morphology [27,28], have been shown to preferentially adsorb and activate CO_2 with the aid of photo-induced electrons [29,30]. In initiating this study, we hypothesized that using TiNT as supports for copper would result in improved behavior in RWGS, as compared to Cu supported on conventional TiO_2 nanopowder (TiNP) In testing this hypothesis, we indeed observed increased activity, but we also observed a complex dependence of the rate on the Cu surface density on the TiNT support that demanded further investigation. Our analysis with *in situ* IR, UV–vis, and X-ray absorption spectroscopies together with DFT calculations lead to the conclusion that surface reconstruction is responsible for the pattern of activity of these materials.

* Corresponding author.
E-mail addresses: weitz@northwestern.edu (E. Weitz), k-gray@northwestern.edu (K.A. Gray), j-notestein@northwestern.edu (J.M. Notestein).

https://doi.org/10.1016/j.apcatb.2019.117754
Received 29 November 2018; Received in revised form 5 April 2019; Accepted 15 May 2019
Available online 16 May 2019
0926-3373/

Table 1
Cu/TiNT properties and catalytic performance.

Material[a]	Surface Area (m^2/g)	Pore Volume (cm^3/g)	Cu Loading (wt%)	Surface Density (Cu/nm^2)	Apparent Activation Energy[b] (kJ/mol)
TiNT	155	0.57	–	–	105
0.3Cu/TiNT	119	0.53	0.4	0.2	65
1.5Cu/TiNT	110	0.51	2.7	1.7	102
3Cu/TiNT	101	0.50	4.5	2.8	98
6Cu/TiNT	94	0.44	9.1	5.6	81

[a] See supporting information Figure S1 and Table S1 for physical properties and apparent barriers over TiNP-based materials.
[b] From the slopes of Fig. 1. Values ± 5 kJ/mol.

2. Experimental

TiO_2 nanotubes (TiNT) were prepared by reconstructing anatase TiO_2 (Sigma, 99.7%, < 25 nm particle size) using a hydrothermal method [31]. The TiNT materials were calcined in a flow of air at 450 °C for 5 h. Cu/TiNP and Cu/TiNT were prepared by incipient wetness impregnation of $Cu(NO_3)_2{\cdot}3H_2O$ (Sigma, 99.999%) on TiO_2 nanopowder (TiNP) and TiNT following a previously described procedure [32], and finally calcined in a flow of air at 450 °C for 4 h. This latter step is expected to collapse the nanotubes somewhat [31], reducing surface areas while retaining the surface termination. The Cu catalysts were prepared with nominal surface densities of 0.3 Cu/nm^2, 1.5 Cu/nm^2, 3 Cu/nm^2 and 6 Cu/nm^2. The latter is denoted, for example, 6Cu/TiNT. Measured Cu loadings and other physical properties are given in Table 1.

Nitrogen adsorption-desorption isotherms were collected using a Micromeritics ASAP 2010 instrument. The elemental compositions of Cu and Ti were determined by a Thermo iCAP 7600 ICP-OES. Raman spectra were collected using a HORIBA LabRAM HR Evolution Confocal Raman with a 785 nm excitation laser. X-ray diffraction (XRD) data were collected using a Rigaku Ultima X-ray diffractometer. Temperature Programmed Reduction (TPR) data were collected using 10% H_2/N_2 as the reductant in an Altamira AMI-200 reactor system over a temperature range of 40–340 °C. *in situ* DRIFTS experiments averaged 64 scans at 4 cm^{-1} resolution from a Nicolet 6700 FTIR spectrometer equipped with a Harrick Praying Mantis diffuse reflectance accessory and an MCT detector.

in situ UV–vis spectra were collected with a Shimadzu UV-3600 spectrometer equipped with a Harrick Praying Mantis diffuse reflectance accessory. The Harrick cell was slightly modified by putting the tip of a thermocouple just under the sample surface, and close to the spot at which spectra were recorded, in order to accurately measure the surface temperature. Barium sulfate (Sigma, 99.998%) was used as the baseline reference for all samples. The sample in the cell was pretreated at 300 °C in Ar for 30 min before any further treatment. *in situ* experiments were performed using H_2 (Airgas, 99.999%) and CO_2 (Airgas, 99.999%) at a flow rate of 20 ml/min at 300 °C.

High-resolution transmission electron micrographs were obtained on a JEOL 2100 F TEM operating at 200 kV. The samples were dispersed in ethanol and drop-cast on a holey carbon-coated Cu grid for imaging.

Periodic plane wave DFT calculations were carried out on anatase TiO_2 modified with Cu as a model for the 0.3 Cu-TiNT system. These were performed using the VASP5.2 code [33,34] with a kinetic energy cut-off of 400 eV. The core-valence interaction was described using the projector augmented wave (PAW) potentials [35,36], with 4 valence electrons for Ti, 6 for O and 11 for Cu. The Perdew-Wang (PW91) approximation to the exchange-correlation functional was used [37]. The TiO_2 anatase (001) substrate was modelled as an 18 atomic layer slab, with a (4× 4) surface supercell expansion (a = 15.324 Å, b = 15.329 Å) and a vacuum gap of 12 Å. This surface was chosen since the anatase (001) facet is characteristic of TiNT and partially collapsed TiNT [27]. Due to the surface supercell expansion used, Γ-point sampling was used and the convergence criteria for the energy and forces were 10^{-4} eV and 0.02 eV. $Å^{-2}$, respectively. All calculations were spin polarized and there were no symmetry restraints applied. Hubbard U corrections were implemented, with U(Ti) = 4.5 eV and U(Cu) = 7 eV, to consistently describe the partially filled Cu 3d states, particularly where Cu^{2+} and reduced Ti^{3+} cations are possible [38,39]. Cation oxidation states were determined from Bader charge analysis and spin mangetisations. To model the different surface modifications, we considered the adsorption and relaxation of a Cu atom and a CuO moiety on anatase (001) and the impact on reducibility and CO_2 adsorption. To this end, different adsorption sites for Cu and CuO were examined and the most stable are shown in the Results and Discussion section.

Catalytic measurements were conducted in a packed-bed tubular stainless-steel reactor (0.25 inch diameter) using 0.1 g catalyst mixed with 0.1 g quartz sand with the same particle size. The catalysts were crushed to particles below 105 microns in order to avoid intraparticle mass transfer limitations. The feed gas mixtures of CO_2 (Airgas, 99.999%), H_2 (Airgas, 99.999%) and He (Airgas, 99.999%) were supplied by mass flow controllers. In each experiment, the catalyst in the reactor was reduced in H_2 at 340 °C for 2 h prior to reacting with 3 MPa of mixtures of CO_2 and H_2 for 3 h at temperatures of 200 °C, 235 °C, 270 °C, 305 °C and 340 °C. Each Cu/TiNP catalyst was tested twice, and each Cu/TiNT catalyst was tested three times. The products were monitored with an online Shimadzu GC-2010, equipped with a Rt-U-BOND column, a Rt-sieve 5A PLOT column, and a TCD detector. CO was the only detected product in all cases. Conversions are kept to < 10% of equilibrium yield for all trials to ensure differential conversion and to minimize the need to correct rates for the approach to equilibrium.

3. Results and discussion

RWGS kinetics were examined in a flow reactor, and CO production rates over the various catalysts are compared in Fig. 1. Fig. 1 only shows a single loading for Cu/TiNP because loading did not have a

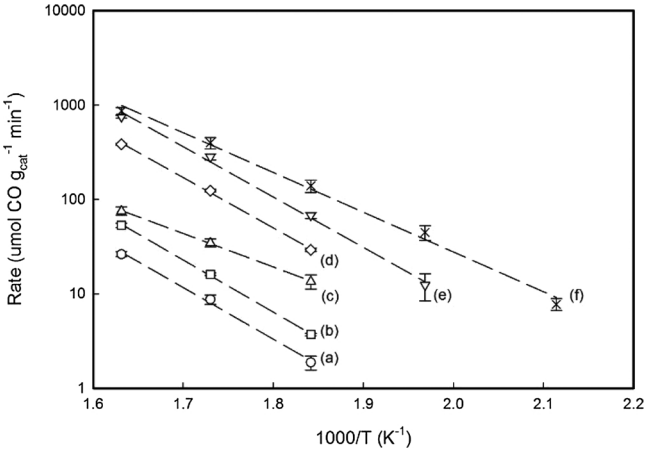

Fig. 1. Arrhenius plots for the reverse water gas shift over (a) 1.5Cu/TiNP as a representative nanoparticle (TiNP) supported catalyst, (b) TiNT, (c) 0.3Cu/TiNT, (d) 1.5Cu/TiNT, (e) 3Cu/TiNT, and (f) 6Cu/TiNT. Reaction conditions: 3 MPa, H_2/CO_2 = 1/1 (v/v), WHSV = 36,000 ml $g_{cat.}^{-1}$ h^{-1}.

significant impact on either CO generation rates (30–65 μmol CO g_{cat}^{-1} min^{-1} at 340 °C) or the apparent activation energies (~100 kJ/mol; Figure S1 and Table S1). However, for Cu/TiNT, the CO production rates were much higher than those over Cu/TiNP and depended significantly on the loading of Cu (50–900 μmol CO g_{cat}^{-1} min^{-1} at 340 °C) when going from ~5% of a monolayer (0.3 Cu/nm^2) to approximately monolayer loading (6 Cu/nm^2). Rates normalized per total Cu loading are given in Figure S2, where 0.3Cu/TiNT shows slightly higher activity than the other Cu/TiNT catalysts, which are similar to each other. Because TiNT has non-negligible activity of its own (Fig. 1) and because the nature of the active site is not immediately known, the discussion is based on rates per gram of total catalyst. The data in Fig. 1 also reveal catalysts with three distinct apparent activation energies (Table 1). Catalysts TiNT, 1.5Cu/TiNT, and 3Cu/TiNT have barriers of ~102 kJ/mol, while that of 6Cu/TiNT is only 81 kJ/mol. The apparent barrier for 0.3 Cu/TiNT is lower still at 65 kJ/mol.

Raman spectra of the as-prepared Cu/TiNT materials are shown in Figure S3. Antase [40] TiO_2 is present in all samples as expected, and crystalline CuO [41] is observed in the 1.5Cu/TiNT, 3Cu/TiNT and 6Cu/TiNT samples.

Normalized TPR profiles of the as-synthesized Cu/TiNT catalysts are plotted from 40 °C to 340 °C in Fig. 2, and the first reduction peak decreased in temperature as the Cu loading increased from 1.5 Cu/nm^2 to 6 Cu/nm^2 (Fig. 2b–d, marked by red arrows). A similar trend has been reported by other researchers [42], and is attributed to the decrease in the portion of strongly-coordinated Cu on TiO_2 as CuO dispersion decreases. Most of the reduction occurred in a characteristic two-step fashion between 160–300 °C, where crystalline CuO supported on TiO_2 typically reduces [42–45]. 0.3 Cu/TiNT is an outlier for this trend, with a relatively low-temperature reduction event. We recently studied very highly dispersed, non-crystalline CuO, such as found in the 0.3 Cu/TiNT (~5% of a monolayer) sample, and observed that the samples became more reducible as loading decreased [46]. This was ascribed to Cu sites being located in highly reactive defects found in very small amounts on support surfaces.

Because of its easy reducibility and low apparent barrier to CO_2 hydrogenation, the structure and reducibility of the species likely present on the surface of the 0.3Cu/TiNT sample were examined in detail with first principles density functional theory simulations. Fig. 3a shows a model structure for this low Cu coverage material, which is composed of an isolated CuO species adsorbed on the anatase (001) surface, the highest energy surface of TiO_2 and the preferred orientation in TiNT [27]. This 0.3Cu/TiNT surface has exclusively Cu^{2+} and Ti^{4+} surface species. Removal of an O atom from the structure in Fig. 3a, to simulate autothermal reduction, requires 1.94 eV, and it produces Ti^{3+} and Cu^{+} in a typical O-Cu-O dumbbell structure (Fig. 3b and c). In contrast, the removal of an O atom to form two Ti^{3+} cations and a Cu^{2+} cation is less stable. In turn, these energies are much lower than the calculated cost of 3.37 eV to remove an O atom from the unmodified anatase (001) surface and generate two Ti^{3+} species within the same computational geometry. Hydrogenation of the surface to give a surface-bound H_2O is significantly exothermic by 1.84 eV (Fig. 3d and e), but as before, this gives a Ti^{3+} and Cu^{+} in a similar structure. See Figure S4 and accompanying text for further details of these calculations. Thus, reduction of CuO-modified anatase (001) is more favourable than the bare anatase (001) and in addition always produces a Cu^{+} and a Ti^{3+} cation, rather than only activating nearby Ti—O—Ti sites. These Cu^{+}/Ti^{3+} sites resulting from H_2 reduction are then models of potential sites for CO_2 adsorption and activation at Ti—O—Cu interfaces.

iIn situ diffuse reflectance UV–vis spectroscopy provides additional information about the speciation of Cu on the surface under reducing pretreatments and with exposure to reactants. In the top panels of Fig. 4, the as-synthesized catalysts were heated to 300 °C under continuous flow of Ar, and the initial spectra were acquired. The gas was switched to H_2 (20 ml/min), and their absorption edges red shifted over

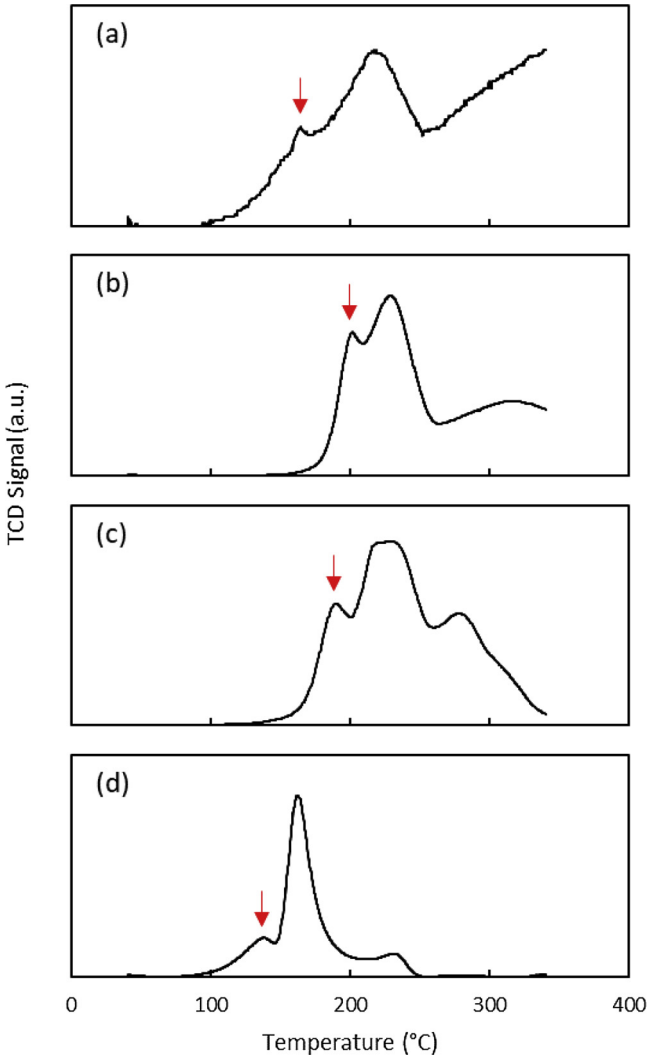

Fig. 2. H_2-TPR profiles of (a) 0.3Cu/TiNT, (b) 1.5Cu/TiNT, (c) 3Cu/TiNT, and (d) 6Cu/TiNT. Signals are nomalized to the maximum intensity feature. Arrows mark the first reduction event. H_2 consumption above 300 °C in (a) arises from the TiNT support itself and becomes proportionally less significant with increasing Cu loading.

10 min due to the reduction of Cu and the TiNT support [47,48]. The characteristic absorption band for metallic Cu nanoparticles, at around 600 nm [49], is discernible for the 1.5Cu/TiNT, 3Cu/TiNT and 6Cu/TiNT samples, but is not for 0.3Cu/TiNT. The assignment of metallic nanoparticles of Cu on these three surfaces is also supported by *ex situ* XRD patterns of the freshly reduced materials (Figure S5) and by TEM of the reduced surfaces (Figure S6). No nanoparticles or crystalline Cu were discernable on the 0.3 Cu/TiNT sample. When the H_2-treated materials were subsequently purged in He and then exposed to CO_2 (20 mL/min) at 300 °C, the absorption bands of the lowest and highest-loaded samples, 0.3Cu/TiNT and 6Cu/TiNT, were blue shifted back to their original state within 5 min, indicating the re-oxidation of Cu by CO_2. In contrast, the absorption bands from metallic Cu on the reduced 1.5Cu/TiNT and 3Cu/TiNT samples were much less changed, even after 30 min exposure to CO_2 at 300 °C. At 300 °C and atmospheric pressure, CO_2 is known to dissociatively adsorb on - and consequently oxidize - metallic Cu surfaces [50–52]. Therefore, the re-oxidation of Cu on 0.3Cu/TiNT and 6Cu/TiNT indicates Cu atoms accessible to CO_2, whereas the persistence of metallic Cu in 1.5Cu/TiNT and 3Cu/TiNT indicates the Cu on those samples is inaccessible to CO_2.

The vibrational modes of surface carbonates derived from CO_2

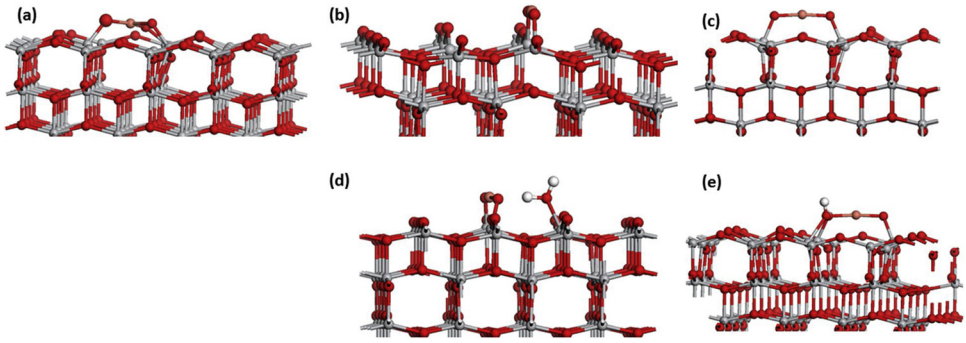

Fig. 3. (a) Atomic structure of a CuO species modifying anatase (001) (b) and (c): atomic structure of CuO-modified anatase (001) after removal of the most stable reducing oxygen vacancy. (d) and (e): atomic structure of CuO-modified anatase (001) after formation of water by H_2 adsorption. (b)/(c) and (d)/(e) show two views of each structure. In this and all figures, Ti is represented by grey spheres, oxygen by red spheres, Cu by brown spheres and H by white spheres (For interpretation of the references to color in this figure legend, the reader is referred to the web version of this article).

chemisorption were next used to probe the TiNT surfaces. Similar to the *in situ* UV–vis studies, the samples were heated to 300 °C under a continuous flow of Ar, reduced in H_2 at 300 °C for 30 min, purged in Ar for 60 min, and background spectra were collected. CO_2 was allowed to flow over the samples for 15 min and the gas was then switched back to Ar to purge the cell of gaseous CO_2. Fig. 5 shows the spectra recorded at 5 min after the gas flow was switched back to Ar. The spectrum obtained on adsorption of CO_2 on TiO_2 nanoparticles (TiNP) is shown in Fig. 5a, where the absorption at 1225 cm^{-1} is attributed to bicarbonate [53], and 1658 cm^{-1} is assigned to the bending mode of water. Both bidentate (1318 cm^{-1}) and monodentate carbonate (1447 and 1379 cm^{-1}) species are observed on TiNP. As a result, CO_2 adsorbed on TiNP has a strong IR absorption from 1800 to 1500 cm^{-1}, owing to the convoluted spectra of bidentate and monodentate carbonate species. However, the spectrum of CO_2 adsorbed on TiNT (Fig. 5b) is dominated by features assigned to water (1616 cm^{-1}) [54,55] and monodenteate carbonate (1521, 1426, and 1374 cm^{-1}) [56].

The spectrum of 0.3Cu/TiNT (Fig. 5c) does not differ significantly from that of TiNT, as expected from the low amounts of Cu present, but one monodentate carbonate peak is red-shifted from 1521 cm^{-1} on TiNT to 1517 cm^{-1} on 0.3Cu/TiNT and another blue shifts from 1426 cm^{-1} on TiNT to 1435 cm^{-1}. These shifts suggest that the monodentate carbonate species were adsorbed on Cu-O-Ti sites of 0.3Cu/TiNT and on Ti-O-Ti sites of TiNT.

Three strong, well-resolved absorption bands at 1635, 1551 (1542), and 1324 (1326) cm^{-1}, are seen with the 1.5Cu/TiNT and 3Cu/TiNT samples (Fig. 5d and e), The absorption at 1635 cm^{-1} is assigned to the bending mode of surface water and is blue-shifted relative to that on 0.3Cu/TiNT or TiNT. This shift is usually attributed to an increase in the concentration of water [57,58]. The latter two bands were identified in our previous study [29] as a bidentate carbonate on TiO_2. For the highest loaded 6Cu/TiNT (Fig. 5f), the IR spectrum more strongly resembles that of low-loading 0.3Cu/TiNT than it does the intermediate loading samples, and the features at 1526 cm^{-1} and 1423 cm^{-1} are

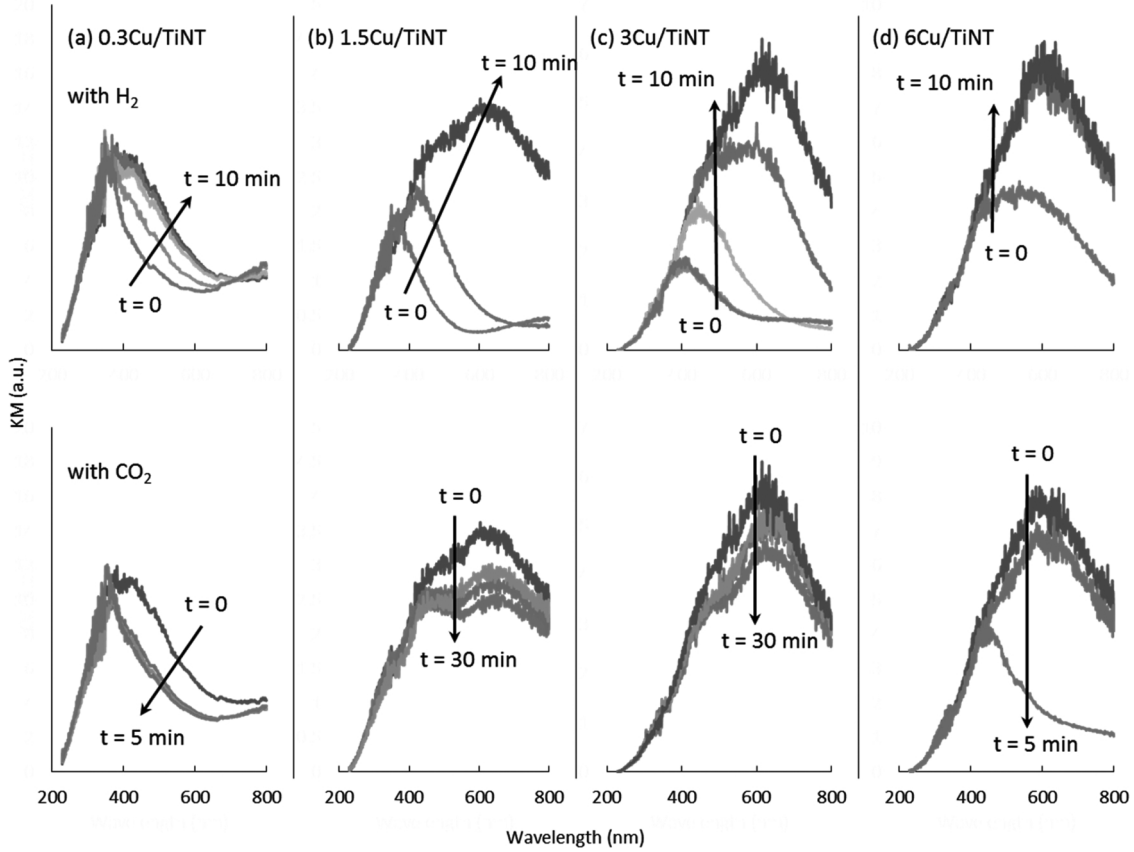

Fig. 4. *in situ* UV–vis spectra of (a) 0.3Cu/TiNT, (b) 1.5Cu/TiNT, (c) 3Cu/TiNT and (d) 6Cu/TiNT at 300 °C. The arrows indicate the increase in time under a continuous flow of H_2 (top panels) and, subsequently, CO_2 (bottom panels).

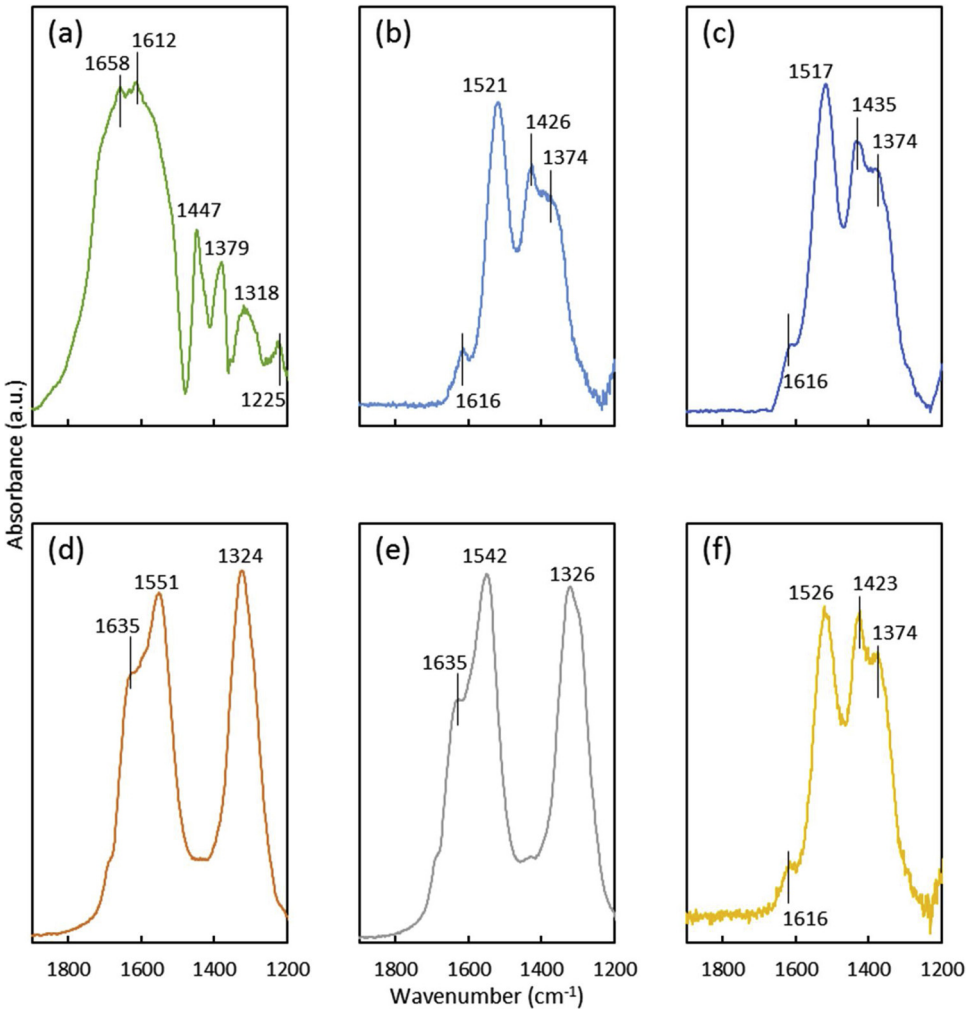

Fig. 5. IR spectra of CO_2 adsorption on the reduced surfaces of (a) TiO_2 nanoparticles (TiNP), (b) TiNT, (c) 0.3Cu/TiNT, (d) 1.5Cu/TiNT, (e) 3Cu/TiNT, and (f) 6Cu/TiNT. Samples were heated to 300 °C under flowing Ar, then H_2, then CO_2. See main text for full experimental conditions.

analogously assigned as monodentate carbonates.

We have also investigated CO_2 adsorption on the reduced surfaces of our computational model of 0.3Cu/TiNT, which shows a number of possible interactions that are consistent with this vibrational spectrum, but which depend on the nature of the oxygen vacancy initially formed. There are three different favorable interaction configurations of CO_2 with reduced 0.3Cu/TiNT, with computed CO_2 adsorption energies of −0.25 eV, −1.04 eV, and −2.50 eV. The two strongest adsorption modes are shown in Fig. 6. Here, the CO_2 adsorbs in an activated form, where C−O bonds elongate and form carbonate-like structures. In all the adsorption geometries, at least one C−O bond forms between the Cu and Ti atoms, again highlighting the key role of the Cu−O−Ti interface at this low coverage of Cu. No significant charge is transferred between the Cu and Ti surface atoms and the CO_2, consistent with initial formation of a carbonate and indicating that the initial reduction of C and re-oxidation of Cu/Ti does not occur spontaneously. This is expected from the overall endothermicity of the RWGS reaction. A more detailed discussion of adsorption geometries is given in Figure S7 and accompanying text. While we observe that the strength of the interaction with CO_2 and that the final structure of the complex between Cu and adsorbed CO_2 depend on which O atom is removed during the initial reduction step, a critical result is that CO_2 adsorption is always preferentially found at the Cu-O-Ti interface. Further studies should address the role of exposed Cu in larger nanoparticles.

We explain the different CO_2 adsorption features on the high/low vs. intermediate loadings of Cu/TiNT catalysts by surface reconstructions akin to a strong metal support interaction (SMSI) [59]. In reducing atmospheres around or above 300 °C, TiO_2 supports are well known to form a non-crystalline, reduced form of SMSI overlayers on supported metals [26,60]. As illustrated in Scheme 1, we propose that SMSI overlayers on 1.5Cu/TiNT and 3Cu/TiNT totally encapsulate the Cu nanoparticle surface after pretreatment in H_2. This prevents the re-oxidation of Cu by CO_2 in the *in situ* UV–vis experiments, and leads to the surface being dominated by a reconstructed TiOx surface distinct from that found on the original TiNT, explaining the changes in the IR spectra. Highly reactive defect sites (e.g. O vacancies) will be more numerous on the SMSI surface than on the bare TiNT surface, explaining the increase in rate absent a change in activation barrier. In contrast, SMSI overlayers do not appear to have completely engulfed the Cu nanoparticles in 6Cu/TiNT, and the exposed interfaces allow the Cu nanoparticles and TiOx SMSI to re-oxidize during *in situ* UV–vis spectroscopy. The inability to form a complete SMSI layer is presumably related to the Cu nanoparticle size, rather than the surface coverage, because TEM (Figure S6) shows ample free TiNT surface and because the DRIFTS spectra of TiNT and 6 Cu/TiNT under CO_2 are similar. Finally, the 0.3Cu/TiNT lacks large Cu nanoparticles (Figure S6), which precludes, by definition, the formation of SMSI overlayers. Therefore, the IR spectra of CO_2 adsorbed on the surfaces of H_2-treated TiNT, 0.3Cu/TiNT and 6Cu/TiNT are all similar and dominated by monodentate carbonate adsorbed at oxidized surfaces similar to those of the original TiNT. Under reaction conditions, these different surfaces (TiNT vs. Cu-O-Ti vs. nanoparticle Cu-TiNT) would lead to different

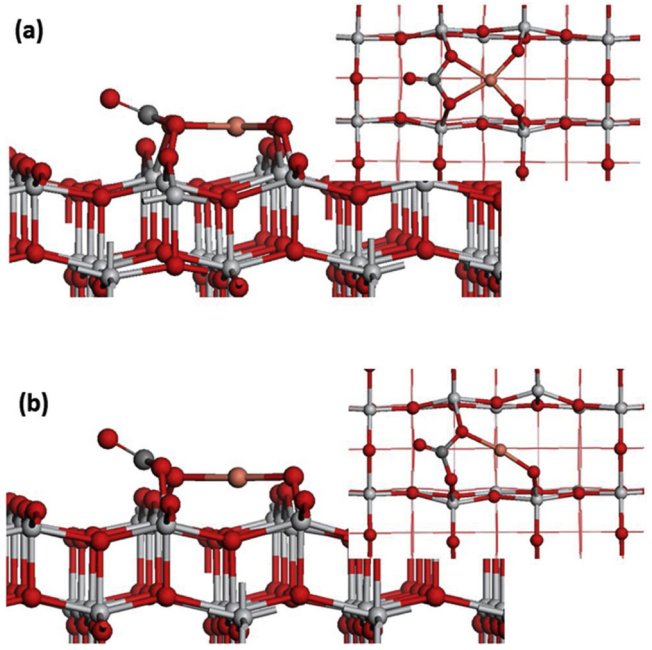

Fig. 6. Side and top views of two possible carbonate-like adsorption modes of CO_2 with models of the reduced surface of 0.3Cu/TiNT (from Fig. 3c). Colour coding is the same as Fig. 3, with carbon shown by the grey sphere.

active sites (e.g. O vacancies) at or near the interface, giving rise to the different apparent observed activation barriers.

After forming the surface carbonates in the procedures corresponding to Fig. 5 and purging the cell with Ar, the samples were re-exposed to H_2 to follow the RWGS reaction and the evolution of new surface species. An example set of spectra for 0.3 Cu/TiNT under sequential Ar, H_2 and Ar flows are shown in Fig. 7, along with the time dependent intensities at 1517 cm^{-1} (monodentate carbonate) and 1616 cm^{-1} (water). The monodentate carbonate species was rapidly depleted under H_2, while surface water was produced at roughly the same rate as the depletion of the monodentate carbonate species. Typical species formed during carbonate hydrogenation [61,62] such as formate (~1580 cm^{-1}) [63], and carboxylate (~1670 cm^{-1}) [64], were not observed. As such, we can propose that the surface monodentate carbonate is the immediate precursor to CO formation.

This correlation between the depletion of surface carbonate and the formation of water was only observed on 0.3Cu/TiNT. On 1.5Cu/TiNT (Fig. 8) and 3Cu/TiNT (Figure S8), both carbonate and water slowly decreased under H_2 and Ar flow. That is likely because the bidentate carbonate species on SMSI surface was converted to monodentate carbonate [29], which was readily depleted in H_2, and further reduction of the SMSI overlayers was unfavorable. Interestingly, the intensities of carbonate on both 6Cu/TiNT (Figure S9) and TiNT (Figure S10) remain nearly unchanged, while the increase of surface adsorbed water under H_2 is attributed to the reaction of H_2 with surface oxygen.

4. Conclusion

It is generally accepted that surface reconstruction plays an important role in creating the active sites of a catalyst. Phenomena such as SMSI are well known in catalysis and extensively studied for supported metals such as Pt [65–67], Pd [68,69], and Au [70]. A SMSI-like overlayer was recently implicated in the catalytic activity of Rh for CO_2 hydrogenation [25]. In the present study, significant changes in apparent activation energy for RWGS were observed as the metal surface density changed for Cu/TiNT catalysts. Specifically, we propose that materials with exposed Cu and TiNT surfaces, either in 0.3Cu/TiNT or 6Cu/TiNT, create catalysts with lower energy barriers than on 1.5Cu/TiNT and 3Cu/TiNT, where Cu is inaccessible to the reactants as a result of SMSI. While unfortunately preventing formation of the lowest-barrier sites, the TiOx created by the SMSI does remain catalytically active. These sites have the same apparent barrier as those in the original TiNT,

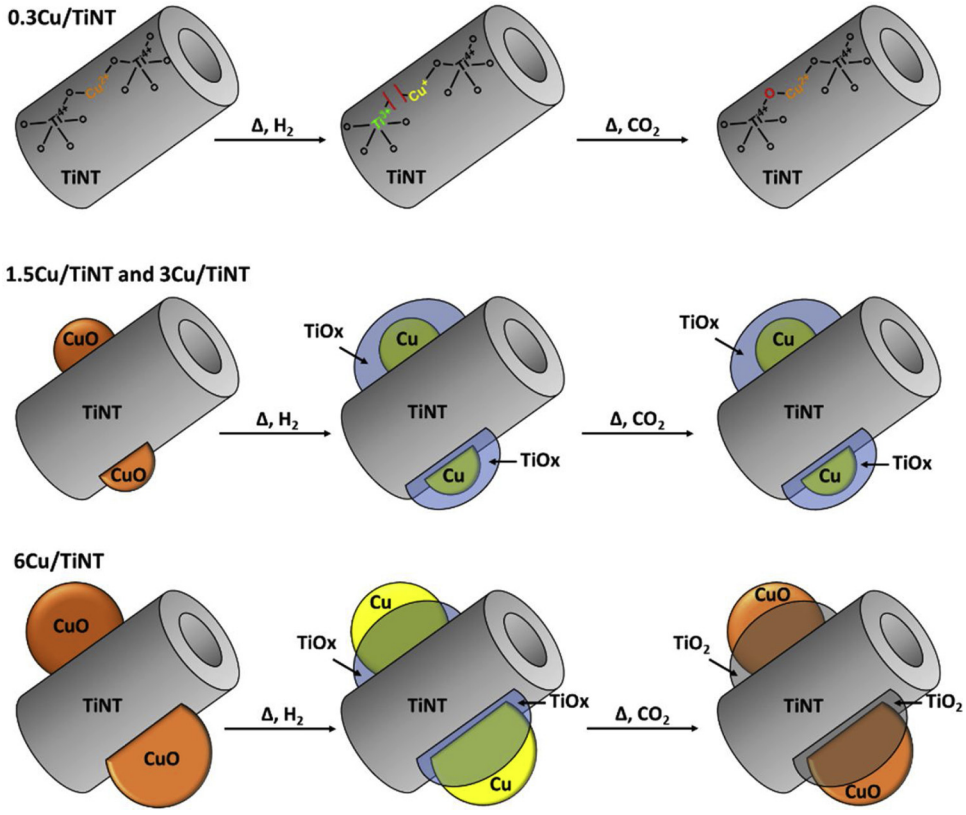

Scheme 1. Surface reconstruction on Cu/TiNT with different Cu loadings. On 0.3Cu/TiNT, oxygen vancancies are created during H_2 treatment and healed by CO_2 and elevated temperature See Figs. 3 and 6 for DFT simulations of such sites. On 1.5Cu/TiNT and 3Cu/TiNT, SMSI overlayers with large numbers of potential RWGS active sites are formed on Cu during H_2 treatment but they prevent Cu from interacting with CO_2 and reoxidizing. On 6Cu/TiNT, overlayers only partially coat Cu during H_2 treatment and Cu remains accesible to CO_2.

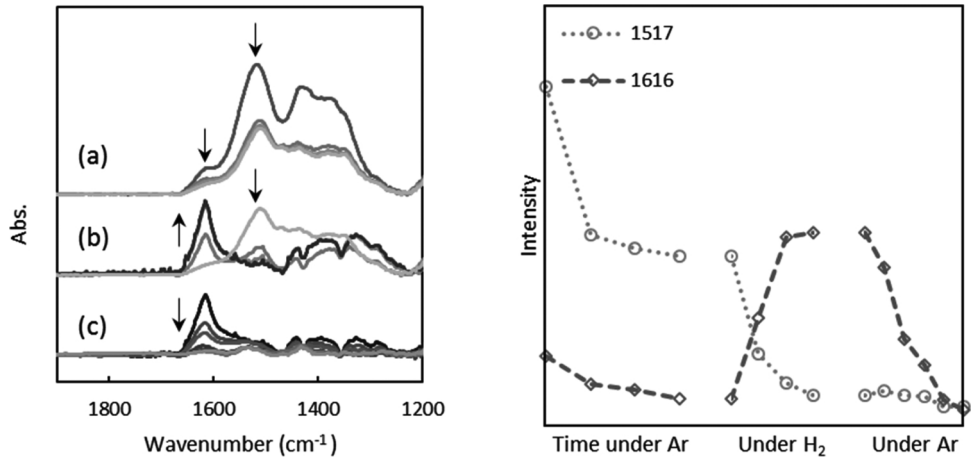

Fig. 7. Left: IR spectra of CO_2 adsorbed 0.3Cu/TiNT under sequential flows of (a) Ar (30 min), (b) H_2 (5 min) and (c) Ar (30 min). Right: The plots of intensities at 1517 and 1616 cm^{-1} versus time.

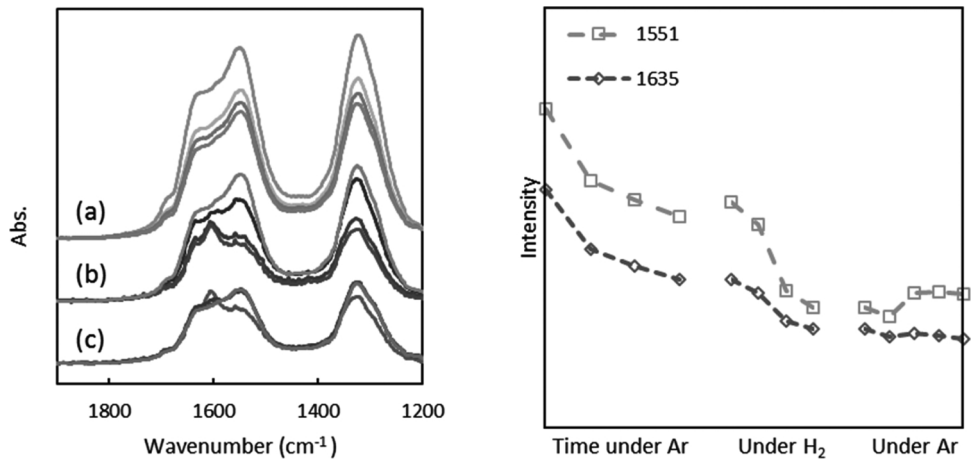

Fig. 8. Left: IR spectra of CO_2 adsorbed 1.5Cu/TiNT under sequential flows of (a) Ar (30 min), (b) H_2 (5 min) and (c) Ar (30 min). Right: The plots of intensities at 1551 and 1635 cm^{-1} versus time.

but appear to be far more numerous. Active sites like O vacancies are presumably rare on the bare titania surfaces, but it is known that thin oxide overlayers have different structures than do the bulk oxides [71]. The increase in activity for all Cu/TiNT samples vs. Cu/TiNP is also likely related to the creation of more O vacancies on the highly-strained and preferentially anatase 001 surfaces of TiNT [27–31]. *in situ* UV–vis and IR spectroscopy show that such SMSI overlayers can form on top of Cu domains after exposure to H_2 at 300 °C. When CO_2 interacts with reduced 1.5Cu/TiNT and 3Cu/TiNT, where the metallic Cu surface is blocked by the SMSI overlayers, bidentate carbonate species are formed. However, when CO_2 interacts with the reduced 0.3Cu/TiNT, Cu assists TiO_2 in CO_2 activation, as supported by DFT calculations. The difference in the activation barriers between 0.3Cu/TiNT and 1.5Cu/TiNT or 3Cu/TiNT suggests an active site may be created at the Cu-O-Ti sites in 0.3Cu/TiNT. The altered actiation barriers indicate that Cu and TiNT surfaces are both involved in CO_2 activation over 6 Cu/TiNT. The exact mechanisms will require further investigation in all cases. This study provides insights for creating effective supported metal catalysts for CO_2 activation and conversion.

Acknowledgements

This research was funded by the National Science Foundation (CBET-1438721). The Department of Energy (DE-FG02-03ER15457) is acknowledged for support of S.L.N. and the CleanCat core facility (DRIFTS and TPR). The Institute for Sustainability and Energy at Northwestern is acknowledged for support of A.G. and for reactor construction. This work made use of the J.B. Cohen X-ray Diffraction Facility and the SPID facility at Northwestern University. These are supported by the MRSEC program of the National Science Foundation (DMR-1121262, DMR-1720139) and the Soft and Hybrid Nanotechnology Experimental (SHyNE) Resource (NSF NNCI-1542205). the International Institute for Nanotechnology (IIN), the Keck Foundation, and the State of Illinois. Metal analysis was performed at the Northwestern University Quantitative Bio-element Imaging Center. M.N. acknowledges support from Science Foundation Ireland through the US-Ireland R&D Partnership program, Grant number SFI/US/14/e2915, access to SFI funded computing resources at Tyndall Institute and the SFI/HEA funded Irish Centre for High End Computing, and support from the COST Action CM1104 “Reducible Metal Oxides, Structure and Function.”

Appendix A. Supplementary data

Supplementary material related to this article can be found, in the online version, at doi:https://doi.org/10.1016/j.apcatb.2019.117754.

References

[1] G. Centi, E.A. Quadrelli, S. Perathoner, Catalysis for CO_2 conversion: a key technology for rapid introduction of renewable energy in the value chain of chemical industries, Energy Environ. Sci. 6 (2013) 1711–1731.

[2] S. Saeidi, N.A.S. Amin, M.R. Rahimpour, Hydrogenation of CO_2 to value-added products—a review and potential future developments, J. Co_2 Util. 5 (2014) 66–81.
[3] M.S. Spencer, On the activation energies of the forward and reverse water-gas shift reaction, Catal. Lett. 32 (1995) 9–13.
[4] D.S. Newsome, The water-gas shift reaction, Catal. Rev. 21 (2006) 275–318.
[5] Y.A. Daza, J.N. Kuhn, CO_2 conversion by reverse water gas shift catalysis: comparison of catalysts, mechanisms and their consequences for CO_2 conversion to liquid fuels, RSC Adv. 6 (2016) 49675–49691.
[6] J. Graciani, et al., Highly active copper-ceria and copper-ceria-Titania catalysts for methanol synthesis from CO_2, Science 345 (2014) 546–550.
[7] I. Toyoshima, G.A. Somorjai, Heats of chemisorption of O_2, H_2, CO, CO_2, and N_2 on polycrystalline and single crystal transition metal surfaces, Catal. Rev. 19 (1979) 105–159.
[8] C.C. Yang, Y.H. Yu, B. van der Linden, J.C. Wu, G. Mul, Artificial photosynthesis over crystalline TiO_2-based catalysts: fact or fiction? J. Am. Chem. Soc. 132 (2010) 8398–8406.
[9] H. Yamashita, Photocatalytic reduction of CO_2 with H_2O on TiO_2 and Cu/TiO_2 catalysts, Res. Chem. Intermed. 20 (1994) 815–823.
[10] T. Tagawa, N. Nomura, M. Shimakage, S. Goto, Effect of supports on copper catalysts for methanol synthesis from CO_2 + H_2, Res. Chem. Intermed. 21 (1995) 193–202.
[11] S.I. In, D.D. Vaughn, R.E. Schaak, Hybrid CuO-$TiO_{2-x}N_x$ hollow nanocubes for photocatalytic conversion of CO_2 into methane under solar irradiation, Angew. Chem. Int. Ed. 51 (2012) 3915–3918.
[12] K.K. Bando, K. Sayama, H. Kusama, K. Okabe, H. Arakawa, In-situ Ft-Ir study on CO_2 hydrogenation over Cu catalysts supported on SiO_2, $Al2O_3$, and TiO_2, Appl. Catal. A 165 (1997) 391–409.
[13] T.C. Schilke, I.A. Fisher, A.T. Bell, Influence of titania on zirconia promoted Cu/SiO_2 catalysts for methanol synthesis from CO/H_2 and CO_2/H_2, Catal. Lett. 54 (1998) 105–111.
[14] M.C. Bradford, C.J. Michael, M. Albert Vannice, The role of metal–support interactions in CO_2 reforming of CH_4, Catal. Today 50 (1999) 87–96.
[15] T.C. Schilke, I.A. Fisher, A.T. Bell, In situ infrared study of methanol synthesis from CO_2/H2on titania and zirconia promoted Cu/SiO_2, J. Catal. 184 (1999) 144–156.
[16] I.H. Tseng, W.-C. Chang, J.C.S. Wu, Photoreduction of CO_2 using sol–gel derived titania and titania-supported copper catalysts, Appl. Catal. B 37 (2002) 37–48.
[17] D. Shi, Y. Feng, S. Zhong, Photocatalytic conversion of CH_4 and CO_2 to oxygenated compounds over Cu/CdS– TiO_2/SiO_2 catalyst, Catal. Today 98 (2004) 505–509.
[18] I.H. Tseng, J.C.S. Wu, H.-Y. Chou, Effects of sol–gel procedures on the photocatalysis of Cu/ TiO_2 in CO_2 photoreduction, J. Catal. 221 (2004) 432–440.
[19] N. Slamet, H. Nasution, E. Purnama, S. Kosela, J. Gunlazuardi, Photocatalytic reduction of CO_2 on copper-doped titania catalysts prepared by improved-impregnation method, Catal. Commun. 6 (2005) 313–319.
[20] B. Srinivas, B. Shubhamangala, K. Lalitha, P. Anil Kumar Reddy, V. Durga Kumari, M. Subrahmanyam, D.B.R. Machiraju, Photocatalytic reduction of CO_2 over Cu-TiO_2/molecular sieve 5A composite, Photochem. Photobiol. 87 (2011) 995–1001.
[21] D. Liu, Y. Fernández, O. Ola, S. Mackintosh, M. Maroto-Valer, C.M.A. Parlett, A.F. Lee, F. Adam, J.C.S. Wu, On the impact of Cu dispersion on CO_2 photoreduction over Cu/TiO_2, Catal. Commun. 25 (2012) 78–82.
[22] L. Liu, F. Gao, H. Zhao, Y. Li, Tailoring Cu valence and oxygen vacancy in Cu/TiO_2 catalysts for enhanced CO_2 photoreduction efficiency, Appl. Catal. B 134-135 (2013) 349–358.
[23] S. Neatu, J.A. Macia-Agullo, P. Concepcion, G. Garcia, Gold-copper nanoalloys supported on TiO_2 as photocatalysts for CO_2 reduction by water, J. Am. Chem. Soc. 136 (2014) 15969–15976.
[24] G.A. Somorjai, Surface reconstruction and catalysis, Annu. Rev. Phys. Chem. 45 (1994) 21–751.
[25] J.C. Matsubu, S. Zhang, L. DeRita, N.S. Marinkovic, J.G. Chen, G.W. Graham, X. Pan, P. Christopher, Adsorbate-mediated strong metal–support interactions in oxide-supported Rh catalysts, Nat. Chem. 9 (2017) 120–127.
[26] J. Strunk, M.A. Bañares, I.E. Wachs, Vibrational spectroscopy of oxide overlayers, Top. Catal. 60 (60) (2017) 1577–1617.
[27] D. Finkelstein-Shapiro, C.Y.H. Tsai, S. Li, K.A. Gray, Synthesis of high-energy anatase nanorods via an intermediate nanotube morphology, Chem. Phys. Lett. 546 (2012) 106–108.
[28] K.C. Schwartzenberg, K.A. Gray, Nanostructured titania: the current and future promise of titania nanotubes, J. Educ. Sci. Technol. 2 (2012) 1617–1624.
[29] W. Wu, K. Bhattacharyya, K.A. Gray, E. Weitz, Photoinduced reactions of surface-bound species on titania nanotubes and platinized titania nanotubes: an in situ FTIR study, J. Phys. Chem. C 117 (2013) 20643–20655.
[30] K. Bhattacharyya, A. Danon, B.K. Vijayan, K.A. Gray, P.C. Stair, E. Weitz, Role of the surface lewis acid and base sites in the adsorption of CO_2 on titania nanotubes and platinized titania nanotubes: an in situ FT-IR study, J. Phys. Chem. C 117 (2013) 12661–12678.
[31] B. Vijayan, N.M. Dimitrijevic, T. Rajh, K.A. Gray, Effect of calcination temperature on the photocatalytic reduction and oxidation processes of hydrothermally synthesized titania nanotubes, J. Phys. Chem. C 114 (2010) 12994–13002.
[32] S.L. Nauert, F. Schax, C. Limberg, J.M. Notestein, Cyclohexane oxidative dehydrogenation over copper oxide catalysts, J. Catal. 341 (2016) 180–190.
[33] G. Kresse, J. Hafner, *Ab initio* molecular-dynamics simulation of the liquid-metal-amorphous-semiconductor transition in germanium, Phys. Rev. B 49 (20) (1994) 14251–14269.
[34] J. Furthmüller, J. Hafner, G. Kresse, Dimer reconstruction and electronic surface states on clean and hydrogenated diamond (100) surfaces, Phys. Rev. B 53 (11) (1996) 7334–7351.
[35] P.E. Blochl, Projector augmented-wave method, Phys. Rev. B 50 (24) (1994) 17953–17979.
[36] G. Kresse, D. Joubert, From ultrasoft pseudopotentials to the projector augmented-wave method, Phys. Rev. B 59 (3) (1999) 1758–1775.
[37] J.P. Perdew, K. Burke, M. Ernzerhof, Generalized gradient approximation made simple, Phys. Rev. Lett. 77 (18) (1996) 3865–3868.
[38] V.I. Anisimov, J. Zaanen, O.K. Andersen, Band theory and Mott insulators: hubbard U instead of stoner I, Phys. Rev. B 44 (3) (1991) 943–954.
[39] S.L. Dudarev, G.A. Botton, S.Y. Savrasov, C.J. Humphreys, A.P. Sutton, Electron-energy-loss spectra and the structural stability of nickel oxide: an LSDA+U study, Phys. Rev. B 57 (3) (1998) 1505–1509.
[40] X. Xue, W. Ji, Z. Mao, H. Mao, Y. Wang, X. Wang, W. Ruan, B. Zhao, J.R. Lombardi, Raman investigation of nanosized TiO_2: effect of crystallite size and quantum confinement, J. Phys. Chem. C 116 (2012) 8792–8797.
[41] F.J. Xu, W.X. Ji, Z. Shen, S.W. Li, H.S. Tang, X. Ye, Z.D. Jia, Q.X. Xin, Raman spectra of CuO nanocrystals, J. Raman Spectrosc. 30 (1999) 413–415.
[42] A. Kubacka, M.J. Muñoz-Batista, M. Fernández-García, S. Obregón, G. Colón, Evolution of H_2 photoproduction with Cu content on CuOx- TiO_2 composite catalysts prepared by a microemulsion method, Appl. Catal. B 163 (2015) 214–222.
[43] H. Zhu, L. Dong, Y. Chen, Effect of titania structure on the properties of its supported copper oxide catalysts, J. Colloid Interface Sci. 357 (2011) 497–503.
[44] G.C. Bond, S.N. Namijo, J.S. Wakeman, Thermal analysis of catalyst precursors: part 2. Influence of support and metal precursor on the reducibility of copper catalysts, J. Mol. Catal. 64 (1991) 305–319.
[45] B. Xu, L. Dong, Y. Chen, Influence of cuo loading on dispersion and reduction behavior of CuO/ TiO_2 (Anatase) system, J. Chem. Soc. Faraday Trans. 94 (1998) 1905–1909.
[46] S.L. Nauert, A.S. Rosen, H. Kim, R.Q. Snurr, P.C. Stair, J.M. Notestein, Evidence for copper dimers in low-loaded CuOx/SiO_2 catalysts for cyclohexane oxidative dehydrogenation, ACS Catal. 8 (2018) 9775–9789.
[47] J. Lee, Y.H. Lee, J.S. Choi, K.S. Park, K.S. Chang, M. Yoon, Hydrothermal synthesis of defective TiO_2 nanoparticles for long-wavelength visible light-photocatalytic killing of cancer cells, RSC Adv. 5 (2015) 99789–99796.
[48] M. Mousavi-Kamazani, Z. Zarghami, R. Rahmatolahzadeh, M. Ramezani, Solvent-free synthesis of Cu-Cu_2O nanocomposites via green thermal decomposition route using novel precursor and investigation of its photocatalytic activity, Adv. Powder Technol. 28 (2017) 2078–2086.
[49] A. Marimuthu, J. Zhang, S. Linic, Tuning selectivity in propylene epoxidation by plasmon mediated photo-switching of Cu oxidation state, Science 339 (2013) 1590–1593.
[50] J. Nakamura, J.A. Rodriguez, C.T. Campbell, Does CO_2 dissociatively adsorb on Cu surfaces? J. Phys. Condens. Matter 1 (1989) SB149–SB160.
[51] F. Muttaqien, Y. Hamamoto, K. Inagaki, Y. Morikawa, Dissociative adsorption of CO_2 on flat, stepped, and kinked Cu surfaces, J. Chem. Phys. 141 (2014) 034702.
[52] B. Eren, R.S. Weatherup, N. Liakakos, G.A. Somorjai, M. Salmeron, Dissociative carbon dioxide adsorption and morphological changes on Cu(100) and Cu(111) at ambient pressures, J. Am. Chem. Soc. 138 (2016) 8207–8211.
[53] G. Busca, V. Lorenzelli, Infrared spectroscopic identification of species arising from reactive adsorption of carbon oxides on metal oxide surfaces, Mater. Chem. 7 (1982) 89–126.
[54] K.S. Finnie, D.J. Cassidy, J.R. Bartlett, J.L. Woolfrey, IR spectroscopy of surface water and Hydroxyl species on nanocrystalline TiO_2 films, Langmuir 17 (2001) 816–820.
[55] K. Tanaka, J.M. White, Characterization of species adsorbed on oxidized and reduced anatase, J. Phys. Chem. 86 (1982) 4708–4714.
[56] A.M. Turek, I.E. Wachs, E. DeCanio, Acidic properties of alumina-supported metal oxide catalysts: an infrared spectroscopy study, J. Phys. Chem. 96 (1992) 5000–5007.
[57] M. Takeuchi, L. Bertinetti, G. Martra, S. Coluccia, M. Anpo, States of H_2O adsorbed on oxides: an investigation by near and mid infrared spectroscopy, Appl. Catal. A Gen. 307 (2006) 13–20.
[58] J. Soria, J. Sanz, I. Sobrados, J.M. Coronado, A.J. Maira, M.D. Hernández-Alonso, F. Fresno, FTIR and NMR study of the adsorbed water on nanocrystalline anatase, J. Phys. Chem. C 111 (2007) 10590–10596.
[59] S.J. Tauster, S.C. Fung, R.T.K. Baker, J.A. Horsley, Strong interactions in supported-metal catalysts, Science 211 (1981) 1121–1125.
[60] S. Zhang, P.N. Plessow, J.J. Willis, S. Dai, M. Xu, G.W. Graham, M. Cargnello, F. Abild-Pedersen, X. Pan, Dynamical observation and detailed description of catalysts under strong metal–Support interaction, Nano Lett. 16 (2016) 4528–4534.
[61] L.C. Grabow, M. Mavrikakis, Mechanism of methanol synthesis on Cu through CO_2 and CO hydrogenation, ACS Catal. 1 (2011) 365–384.
[62] F. Studt, et al., The mechanism of CO and CO_2 hydrogenation to methanol over Cu-Based catalysts, ChemCatChem 7 (2015) 1105–1111.
[63] D.H. Gibson, Carbon dioxide coordination chemistry: metal complexes and surface-bound species. What relationships? Coord. Chem. Rev. 185-186 (1999) 335–355.
[64] W. Su, J. Zhang, Z. Feng, T. Chen, P. Ying, C. Li, Surface phases of TiO_2 nanoparticles studied by UV Raman spectroscopy and FT-IR spectroscopy, J. Phys. Chem. C 112 (2008) 7710–7716.
[65] S.C. Fung, Xps studies of strong metal-support interactions (SMSI)—PtTiO_2, J. Catal. 76 (1982) 225–230.
[66] A.K. Datye, D.S. Kalakkad, M.H. Yao, D.J. Smith, Comparison of metal-support interactions in Pt/ TiO_2 and Pt/CeO_2, J. Catal. 155 (1995) 148–153.
[67] O. Dulub, W. Hebenstreit, U. Diebold, Imaging cluster surfaces with atomic resolution: the strong metal-support interaction state of Pt supported on TiO_2 (110), Phys. Rev. Lett. 84 (2000) 3646–3649.
[68] M.A. Vannice, S.Y. Wang, S.H. Moon, The effect of SMSI (Strong metal-support interaction) behavior on CO adsorption and hydrogenation on Pd catalysts: I. IR

spectra of adsorbed CO prior to and during reaction conditions, J. Catal. 71 (1981) 152–166.
[69] M.S. Kim, S.H. Chung, C.J. Yoo, M.S. Lee, I.H. Cho, D.W. Lee, K.Y. Lee, Catalytic reduction of nitrate in water over Pd–Cu/ TiO_2 catalyst: effect of the strong metal-support interaction (SMSI) on the catalytic activity, Appl. Catal. B 142-143 (2013) 354–361.
[70] H. Tang, et al., Classical strong metal–support interactions between gold nanoparticles and titanium dioxide, Sci. Adv. 3 (2017).
[71] H.V. Thang, S. Tosoni, G. Pacchioni, Evidence of Charge Transfer to Atomic and Molecular Adsorbates on ZnO/X(111) (X = Cu, Ag, Au) Ultrathin Films. Relevance for Cu/ZnO Catalysts, ACS Catal. 8 (2018) 4110–4119.